

# FREQUENCY DOMAIN BLIND DECONVOLUTION IN MULTIFRAME IMAGING USING ANISOTROPIC SPATIALLY-ADAPTIVE DENOISING

*Vladimir Katkovnik, Dmitriy Paliy, Karen Egiazarian, and Jaakko Astola*

Institute of Signal Processing, Tampere University of Technology, P.O.Box 553, FIN-33101, Tampere, Finland  
e-mail: firstname.lastname@tut.fi

## ABSTRACT

In this paper we present a novel method for multiframe blind deblurring of noisy images. It is based on minimization of the energy criterion produced in the frequency domain using a recursive gradient-projection algorithm. For filtering and regularization we use the local polynomial approximation (LPA) of both the image and blur operators, and paradigm of the intersection of confidence intervals (ICI) applied for selection adaptively varying scales (window sizes) of LPA. The LPA-ICI algorithm is nonlinear and spatially-adaptive with respect to the smoothness and irregularities of the image and blur operators. Simulation experiments demonstrate efficiency and good performance of the proposed deconvolution technique.

## 1. INTRODUCTION

Image processing based on multiple observations of one scene aims to enhance comprehensive restoration quality, often when knowledge about image formation is incomplete. Classical fields of application are the astronomy, remote sensing, medical imaging, etc. Multisensor data of different spatial, temporal, and spectral resolutions are exploited for image sharpening, improvement of registration accuracy, feature enhancement, and improved classification. Other examples can be seen in digital microscopy, where the same specimen may be recorded at several different focus settings; or in multispectral radar imaging through a scattering medium which has different transfer functions at different frequencies.

Image restoration is an inverse problem which assumes having a prior information about the formation model. This model includes all sorts of distortions related to the image degradation. For instance, the atmospheric turbulence, the relative motion between an object and the camera, the out-of-focus camera, the variations in optical and electronic imaging components, etc.

Conventionally, the image acquisition is modelled by the convolution with the point-spread function (PSF) and noise. The PSF introduces low-pass distortions into an image which are called often as blur. When the blur is unknown, the image restoration becomes a blind inverse problem or blind deconvolution. For multiple observations of one scene, it is a multiframe, or multichannel, blind inverse problem.

A theoretical breakthrough on the blind and non-blind deconvolution techniques has been done in works on perfect blur and image reconstruction. With the blur functions satisfying certain co-primeness requirements the existence and uniqueness of the solution is guaranteed under quite unrestrictive conditions, i.e. both the blur and the original image can be determined exactly in the absence of noise, and stably estimated in its presence [1, 2, 3].

A number of works have been done to deal with noisy data. In particular, the blind deconvolution based on the Bussgang filters is proposed in [4]. The inverse filter is build as a nonlinear approximation of the optimal Wiener deconvolution filter.

Blind noise-resistant deconvolution algorithms based on the least square method has been proposed in [5]. The criterion includes the standard quadratic fidelity term as well as a quadratic term of the cross-channel balance. Overall, the criterion is nonquadratic as the total variation (TV) and Mumford-Shah energy functionals are used as the regularizers. These nonquadratic terms, or penalty functions, of the criterion result in a nonlinear edge-preserving filtering [7, 8, 9]. It is shown in [5] that the proposed algorithm using this sort of regularization performs quite well.

The novel approach obtained as a further development of [5] was proposed in the recent paper [6]. The main emphasize of this work is done on multichannel deblurring of spatially misaligned images. The proposed algorithm does not require the accurate size of supports of blur functions, and the observed images are not supposed to be perfectly spatially aligned.

The technique proposed in this paper is based on the frequency domain representation of the observation model. One of the benefits of this approach concerns the ability to work with large images and with large supports of PSFs. The recursive procedure completed by the spatially-adaptive LPA-ICI filters works as a spatially-adaptive regularizer for the blur-operator inversion. For non-blind image deconvolution this spatially-adaptive LPA-ICI inverse has been presented in [10].

Simulation experiments show the efficiency of the restoration algorithm which demonstrates good convergence and high quality image restoration. The algorithm is quite robust with respect to the support sizes used in the PSF estimation.

## 2. OBSERVATION MODEL

Consider a 2D single-input multiple-output (SIMO) linear spatially invariant imaging system. Such a system is appropriate for the model of multiple cameras, multiple focuses of a single camera, or acquisition of images from a single camera through a changing medium. The input to this system is an unknown image  $y(x)$ ,  $x \in X$ , where  $X = \{x_1, x_2 : x_1 = 1, 2, \dots, n_1, x_2 = 1, 2, \dots, n_2\}$ , of the size  $n_1 \times n_2$ . This image is distorted by unknown finite impulse response functions modelled by the PSFs  $v_j(x)$ ,  $j = 1, \dots, L$ . It is assumed that  $v_j(x)$  are discrete spatially invariant. The discrete convolutions of the input  $y(x)$  and the PSFs  $v_j(x)$  are degraded by the additive white Gaussian noise to produce the observed output images:

$$z_j(x) = (y \otimes v_j)(x) + \sigma_j \eta_j(x), \quad j = 1, \dots, L. \quad (1)$$

It is assumed that the noise in each channel is uncorrelated with the noise from other channels and  $\eta_j(x)$  have the Gaussian distribution  $\mathcal{N}(0, 1)$ . The parameters  $\sigma_j$  are the standard deviations of the noise in the channels.

The problem is to reconstruct both the image  $y$  and the PSFs  $v_j$  from the observations  $\{z_j(x) : x \in X, j = 1, \dots, L\}$ .

### 3. GRADIENT-PROJECTION ALGORITHM

Using the Parseval theorem,  $\sum_x y^2(x) = \sum_f |Y(f)|^2 / (n_1 n_2)$ , we introduce the following basic quadratic criterion loss-function:

$$J = \sum_{j=1}^L \frac{1}{\sigma_j^2} \sum_f |Z_j - Y V_j|^2 + \lambda_2 \sum_f |Y|^2 + \lambda_1 \sum_{i,j=1}^L d_{ij} \sum_f |Z_i V_j - Z_j V_i|^2 + \lambda_3 \sum_{j=1}^L \sum_f |V_j|^2, \quad (2)$$

where

$$d_{ij} = \frac{n_1 n_2}{\sigma_i^2 \sum_f |V_j|^2 + \sigma_j^2 \sum_f |V_i|^2}. \quad (3)$$

Here,  $Z_j(f)$ ,  $Y(f)$ , and  $V_j(f)$  are the Fourier transforms (FTs) of the signals  $z_j(x)$ ,  $y(x)$ , and  $v_j(x)$ , respectively. For the sake of simplicity, we do not show in the formulas the frequency argument  $f$ . The symbol  $\mathcal{F}\{\cdot\}$  is used for the Fourier transform.

The necessary unconstrained minimum conditions for  $z$  can be written as  $\partial_{Y^*} J = 0$ ,  $\partial_{V_j^*} J = 0$ ,  $j = 1, \dots, L$ , for any frequency  $f$ . Considering  $d_{ij}$  as a constant parameter, we find after elementary manipulations that

$$\partial_{Y^*} J = - \sum_{j=1}^L \frac{1}{\sigma_j^2} (Z_j - V_j Y) V_j^* + \lambda_2 Y, \quad (4)$$

$$\partial_{V_j^*} J = - \frac{1}{\sigma_j^2} (Z_j - V_j Y) Y^* + \lambda_1 \sum_{i,j=1, i \neq j}^L d_{ij} (Z_i V_j - Z_j V_i) Z_i^* + \lambda_3 \sum_{j=1}^L V_j, \quad (5)$$

where the star (\*) stays for the complex-conjugate variable.

The estimates of the signal and the PSFs are solutions of the following problem:

$$(\hat{y}, \hat{v}) = \arg \min_{y \in Q_y, v_j \in Q_{v_j}} J, \quad (6)$$

where the admissible convex sets  $Q_y$  for  $y$  and  $Q_{v_j}$  for  $v_j$  are defined as  $Q_y = \{y : 0 \leq y \leq 1\}$ ,  $Q_{v_j} = \{v_j : \sum_x v_j(x) = 1, v_j(x) \geq 0, v_j(x) = 0 \text{ if } |x_1| > \Delta, |x_2| > \Delta\}$ . The sets  $Q_{v_j}$  impose the positivity and normalized mean value assumptions on PSFs  $v_j$ . The parameter  $\Delta > 0$  defines the size of the support of  $v_j(x)$ .

The recursive projection gradient algorithm is used for solution of (6). Firstly, the values  $Y^{(k)}$  and  $V_j^{(k)}$  are calculated:

$$Y^{(k)} = Y^{(k-1)} - \alpha_k \partial_{Y^*} J(Y^{(k-1)}, V^{(k-1)}), \quad (7)$$

$$V_j^{(k)} = V_j^{(k-1)} - \beta_k \partial_{V_j^*} J(Y^{(k)}, V^{(k-1)}), \quad (8)$$

where  $k = 1, \dots$ ;  $\alpha_k > 0$  and  $\beta_k > 0$  are step-size parameters. The corresponding gradient components are given in (4)-(5).

Secondly,  $Y^{(k)}$ ,  $V_j^{(k)}$  are projected onto the sets  $Q_y$ ,  $Q_{v_j}$ :

$$P_{Q_y}\{y\} = \max\{0, \min(1, y)\}, \quad (9)$$

$$P_{Q_{v_j}}\{v_j\} = v_j / \sum_x v_j(x), \quad v_j \geq 0, \quad (10)$$

$$v_j(x) = 0 \text{ if } |x_1| > \Delta, |x_2| > \Delta.$$

The initialization  $(Y^{(0)}, V_j^{(0)})$  is assumed in (7)-(8). The normalization of the PSFs can be done in the frequency

domain by replacing  $V_j^{(k)}$  on  $V_j^{(k)}/V_j^{(k)}(0)$ , as  $V_j^{(k)}(0) = \sum_x v_j^{(k)}(x)$ , where  $v_j^{(k)}(x) = \mathcal{F}^{-1}\{V_j^{(k)}(f)\}$ .

The projection on  $Q_y$  requires the inverse FT  $y^{(k)}(x) = \mathcal{F}^{-1}\{Y^{(k)}(f)\}$  with the projection of  $y^{(k)}(x)$  calculated according to (9).

The ill-conditioning of the considered inverse problem means that the criterion  $J$  has different scale behavior for different frequencies. In order to enable stable iterations for all frequencies the step-sizes  $\alpha_k$  and  $\beta_k$  should be small and, as result, the partial convergence rates on  $Y^{(k)}$  and  $V_j^{(k)}$  can be very slow.

For the considered frequency domain calculations, a behavior of the algorithm on the variables  $Y$  and  $V_j$  is defined mainly by the second order derivative  $H_{Y^*Y} = \partial_{Y^*} \partial_{Y^*} J$  for  $Y$  and the Hessian matrix  $H_{V^*V} = \left( \partial_{V_i^*} \partial_{V_j^*} J \right)_{i,j}$  for  $V$ .

The convergence rate of the algorithm (7)-(8) can be essentially improved using the diagonal terms of the Hessian matrix  $H_{Y^*Y}$  and  $H_{V^*V}$  as scaling factors of the step sizes:

$$Y^{(k)} = P_{Q_y} \left\{ Y^{(k-1)} - \alpha_k \frac{1}{H_{Y^*Y}} \partial_{Y^*} J(Y^{(k)}, V^{(k)}) \right\}, \quad (11)$$

$$V_j^{(k)} = P_{Q_{v_j}} \left\{ V_j^{(k-1)} - \beta_k \frac{1}{H_{V_j^*V_j}} \partial_{V_j^*} J(Y^{(k)}, V^{(k)}) \right\}, \quad (12)$$

where  $H_{Y^*Y} = \sum_j \frac{1}{\sigma_j^2} |V_j|^2 + \lambda_2$  and  $H_{V_j^*V_j} = \frac{1}{\sigma_j^2} |Y|^2 + \lambda_1 \sum_{i,i \neq j} d_{ij} |Z_i|^2 + \lambda_3$ .

Substitution of  $H_{Y^*Y}$  and  $H_{V_j^*V_j}$  into (11)-(12) gives the following final formulas for the iterations:

$$Y^{(k)} = P_{Q_y} \left\{ (1 - \alpha_k) Y^{(k-1)} + \alpha_k \frac{\sum_j Z_j V_j^{*(k-1)} / \sigma_j^2}{\sum_j |V_j^{(k-1)}|^2 / \sigma_j^2 + \lambda_2} \right\}, \quad (13)$$

$$V_j^{(k)} = P_{Q_{v_j}} \left\{ (1 - \beta_k) V_j^{(k-1)} + \beta_k \frac{Z_j Y^{*(k-1)} / \sigma_j^2 + \lambda_1 Z_j \sum_{i,i \neq j} d_{ij}^{(k-1)} V_i^{(k-1)} Z_i^*}{|Y^{(k)}|^2 / \sigma_j^2 + \lambda_1 \sum_{i,i \neq j} d_{ij}^{(k-1)} |Z_i|^2 + \lambda_3} \right\}, \quad (14)$$

where  $d_{ij}^{(k-1)}$  are calculated in (3) for  $V_j = V_j^{(k-1)}$ .

Some of the restrictions defining  $Q_y$  and  $Q_{v_j}$  are not principal and imposed only in order to improve the convergence and the accuracy of the algorithm. In particular it concerns the requirement  $0 \leq y \leq 1$ .

### 4. LPA-ICI ADAPTIVE DENOISING

The adaptive LPA-ICI filtering algorithm is described in a number of publications [10, 11]. It forms a bank of the directional linear filters with kernels  $g_{h,\theta}$  obtained by LPA. A rotated directional nonsymmetric kernel  $g_{h,\theta}$  is used with the angle  $\theta$  which defines the directionality of the filter, and  $h$  as a length of the kernel support (or a scale parameter of the kernel) in this direction. The directionality of the kernel is defined by the non-symmetric window-function used in the LPA. The directional estimates are calculated using the convolutions  $\hat{y}_{h,\theta}(x) = (g_{h,\theta} \otimes z_j)(x)$  or, in the frequency domain, as the products of the corresponding FTs:  $G_{h,\theta}(f) \cdot Z_j(f)$ , where  $G_{h,\theta} = \mathcal{F}\{g_{h,\theta}\}$ .

The non-linearity of the adaptive filtering is incorporated into the ICI rule. This ICI is the algorithm for selection of the adaptive scale parameter  $h$  for every estimation pixel  $x$ . The estimates  $\hat{y}_{h,\theta}(x)$  are calculated for a grid of

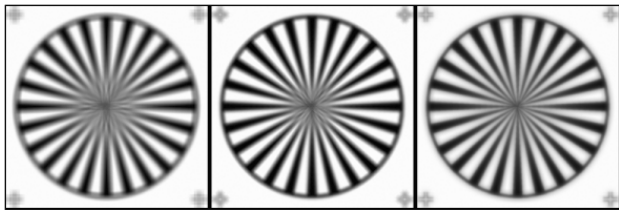


Figure 1: Observations of the noisy blurred "Testpat1" images.



Figure 2: Initial guess, calculated as the mean of the three observed images, the estimate and estimation errors.

$h \in H = \{h_1, h_2, \dots, h_J\}$ , where  $h_1 < h_2 < \dots < h_J$ . The adaptive scale is defined as the largest  $h^+$  of those scales in  $H$  which estimate does not differ significantly from the estimates corresponding to the smaller window sizes.

This common idea is implemented as follows. We consider a sequence of confidence intervals  $D_s = [\hat{y}_{h_s, \theta}(x) - \Gamma \sigma_{\hat{y}_{h_s, \theta}}, \hat{y}_{h_s, \theta}(x) + \Gamma \sigma_{\hat{y}_{h_s, \theta}}]$ ,  $s = 1, \dots, J$ , where  $\Gamma > 0$  is a parameter and  $\sigma_{\hat{y}_{h_s, \theta}}$  is standard deviation of the estimate  $\hat{y}_{h_s, \theta}$  computed as  $\sigma_{\hat{y}_{h_s, \theta}} = \sigma \sqrt{\sum_x g_{h_s, \theta}^2(x)}$ .

The ICI rule is stated as follows: consider the intersection of the confidence intervals  $I_s = \bigcap_{i=1}^s D_i$  and let  $s^+$  be the largest of the indices  $s$  for which  $I_s$  is non-empty. Then the optimal scale  $h^+$  is defined as  $h^+ = h_{s^+}$  and, as result, the optimal scale estimate is  $\hat{y}_{h^+, \theta}(x)$ .

The parameter  $\Gamma$  is a key element of the algorithm as it says when a difference between estimate deviations is large or small. Too large value of this parameter leads to signal oversmoothing and too small value leads to undersmoothing. In this paper we treat  $\Gamma$  as a fixed design parameter.

Optimization of  $h$  for each of the sector estimates yields the adaptive scales  $h^+(\theta)$  for each direction  $\theta$ . The union of the supports of  $g_{h^+(\theta), \theta}$  is considered as an approximation of the best local vicinity of  $x$  in which the estimation model fits the data. The final estimate is calculated as a linear combination of the obtained adaptive directional estimates  $\hat{y}_{h^+, \theta}(x)$ .

It is convenient to treat this complex LPA-ICI multidirectional algorithm as an adaptive filter with two inputs  $z$  and  $\sigma$ , and the one output  $\hat{y}$ . The input-output equation can be written as  $\hat{y} = \mathcal{LI}\{z, \sigma\}$  by denoting the calculations imbedded in this algorithm as an  $\mathcal{LI}$  operator.

## 5. BLIND DECONVOLUTION ALGORITHM

Now we are in a position to describe the developed blind multichannel deconvolution algorithm.

1. *Initialization*: We use the Gaussian density for  $v_j^{(0)}$  and the mean of the observed images  $y^{(0)} = \sum_{j=1}^L z_j(x)/L$  as the initial estimates.
2. *Image estimation*: Calculate  $Y^{(k)}$  according to (13) without projection.

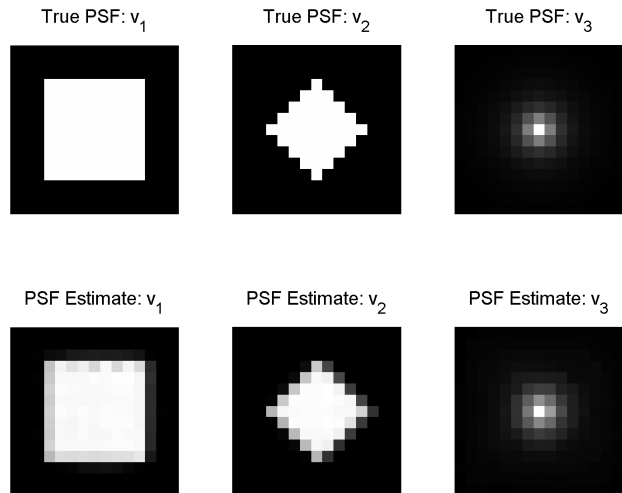


Figure 3: The estimates and true PSFs of the three channel imaging system

3. *Image filtering*: Filter  $Y^{(k)}$  by the LPA-ICI algorithm as following.

- 3a. Calculate the inverse FT  $y^{(k)} = \mathcal{F}^{-1}\{Y^{(k)}\}$ .
- 3b. Calculate the estimate of the standard deviation  $\sigma_{y^{(k)}}$  of the noise in  $y^{(k)}$  using the median estimate of the signal's differences (e.g. [10, 11]).
- 3c. Filter  $y^{(k)}$  according to the algorithm:  $y^{(k)} \triangleq \mathcal{LI}\{y^{(k)}, \sigma_{y^{(k)}}\}$ .

4. *Image projection*:

- 4a. Project  $y^{(k)}$  onto the segment  $[0, 1]$ ,  $y^{(k)} \triangleq P_{Q_y}\{y^{(k)}\}$ , according to (9).
- 4b. Calculate  $Y^{(k)} = \mathcal{F}\{y^{(k)}\}$ .

5. *PSF estimation*: Calculate  $V_j^{(k)}$  according to (14) without filtering and projection. Repeat these calculations  $K_{int}$  times. This internal iterations imbedded in the main recursive algorithm are used to accelerate the convergence rate of the algorithm.

6. *PSF projection*:

- 6a. Calculate  $v_j^{(k)} = \mathcal{F}^{-1}\{V_j^{(k)}\}$ .
- 6b. Project the PSFs estimates  $v_j^{(k)} \triangleq P_{Q_{v_j}}\{v_j^{(k)}\}$  according to (10).

7. *PSF filtering*: Filter  $v_j^{(k)}$  by the LPA-ICI algorithm:

- 7a. Calculate the standard deviation of the noise in  $v_j^{(k)}$  similarly to (3c).
- 7b. Filter  $v_j^{(k)}$  according to the algorithm:  $v_j^{(k)} \triangleq \mathcal{LI}\{v_j^{(k)}, \sigma_{v_j^{(k)}}\}$ ,  $j = 1, \dots, L$ .

8. *Increase  $k$  and repeat steps (2) – (8)  $K$  times.*

Note that the LPA-ICI filtering-regularization is embedded in the recursive algorithm introduced originally in the form (13)-(14). This LPA-ICI filtering is produced in the spatial domain and requires the backward and forward FT of the frequency domain estimates  $V_j^{(k)}$ ,  $Y^{(k)}$ . Operations in the frequency domain (13)-(14) do not impose restrictions on the support size of PSFs  $v_j$ . However, the projection  $P_{Q_{v_j}}\{v_j^{(k)}\}$  means that the maximal size of PSFs  $v_j^{(k)}$  does not exceed a fixed value, which is  $15 \times 15$  in simulation results

BSNR	<i>Cameraman</i>		<i>Lena</i>		<i>Testpat</i>		<i>Text</i>		<i>Boats</i>	
	PSNR	MAE	PSNR	MAE	PSNR	MAE	PSNR	MAE	PSNR	MAE
20	24.6	8.79	26.12	8.44	19.5	16.0	22.8	7.86	26.6	8.14
30	28.8	5.55	31.1	4.90	24.2	8.57	32.0	2.65	31.2	5.11
40	33.0	3.73	35.7	3.05	25.7	5.75	36.6	1.19	34.8	3.49
50	38.7	2.17	38.7	2.15	38.0	1.66	37.6	0.90	36.9	2.75

Table 1: PSNR and MAE criteria values for the deblurred grayscale estimates.

given in the next section. The reduced size of PSF reduces the amount of necessary computations.

## 6. SIMULATION EXPERIMENTS

### 6.1 Restoration of grayscale images

We consider three channel observations with the following different PSFs: Box-car  $9 \times 9$  uniform; Box-car  $7 \times 7$  uniform rotated by  $45^\circ$ ; "Inverse-quadratic"  $v(x_1, x_2) = (1 + x_1^2 + x_2^2)^{-1}$ ,  $x_1, x_2 = -7, \dots, 7$  (Fig.3). The level of noise in the observations  $z_j$ ,  $j = 1, 2, 3$ , is such that the blurred signal-to-noise ratio (BSNR)  $\text{BSNR} = 10 \log_{10} \left( \frac{1}{n_1 n_2 \sigma_j^2} \left\| (y \otimes v_j)(x) - \frac{1}{n_1 n_2} \sum_{\bar{x}} (y \otimes v_j)(x) \right\|_2^2 \right)$  is equal to 20, 30, 40 or 50 dB.

The narrow directional supports of the LPA kernels  $g_{h,\theta}$  are defined by the two-dimensional scale  $h = (h_1, h_2)$  with  $h_1$  and  $h_2$  defining the length and the width of the kernels respectively.

For image filtering these supports are line-wise given by the set  $H = \{(1, 1), (2, 1), (3, 1), (5, 1), (7, 1), (11, 1)\}$ . All these kernels have the width  $h_2 = 1$ . For the PSF we use quadrant support kernels with equal lengths and widths  $H = \{(1, 1), (2, 2), (3, 3), (5, 5), (7, 7), (11, 11)\}$ . The zero order LPA with uniform window functions is used for  $g_{h,\theta}$ . Thus, all the estimates are calculated as the sample mean of observations included in the kernel supports.

For the image the estimates and the adaptive scales  $h_\theta^+(x)$  are calculated for eight directions  $\theta(i) = (i-1)\pi/4$ ,  $i = 1, \dots, 8$ , with the parameter  $\Gamma = 0.9$ . For the PSFs the estimates and the adaptive scales  $h_\theta^+(x)$  are calculated for four directions  $\theta(i) = (i-1)\pi/2$ ,  $i = 1, \dots, 4$ , with the parameter  $\Gamma = 1.5$ .

These ICI adaptive directional estimates are aggregated in the final one using the weighted mean of the directional estimates with the weights equal to the inverse variances of these estimates [10],[11].

Observations of the  $256 \times 256$  image "Testpat" image corrupted by an additive zero-mean Gaussian noise (BSNR=40 dB) are shown in Fig.1. The initial guess as well as the estimate and the estimation errors are shown in Fig.2. We may note that the reconstruction is nearly perfect, in particular in the difficult central part at the image.

The developed frequency domain technique can be used without restrictions on the size of the supports of the PSFs. However, even quite approximate information about the maximal sizes of the PSFs improves the convergence rate as well as the quality of image and PSFs restoration. We assume that the supports of PSFs  $v_j$  do not exceed size  $15 \times 15$ . This step is important also from the viewpoint of reducing computational cost of the iterative scheme.

The parameter  $\lambda_1$  balancing the fidelity and the channel equalization terms is a design parameter of the algorithm and essentially affects the accuracy. It is fixed to be equal to 1.2 in the scheme. It follows from the experiments that the influence of the regularization parameters  $\lambda_2$  and  $\lambda_3$  is insignificant and we fix them to be equal to  $10^{-7}$ . It has been found for various scenarios that good results are obtained for  $\alpha_k = 0.6$  and  $\beta_k = 0.9$ . The total number of iterations in

the algorithm  $K$  is fixed to be 20. The number of internal iterations  $K_{int}$  is fixed to be 7.

The true three PSFs and their estimates obtained for *Testpat* image are shown in Fig.3. It is clearly seen that they are well-restored despite of some minor artefacts.

The blurring effects given by the used PSFs are significant, as it can be seen in Fig.1. Nevertheless, for the well-known test images used in our experiments the restoration is very good.

The numerical evaluation can be seen in Table 1 for a variety of standard test grayscale images and noise settings. All of the images of the sizes  $256 \times 256$  except *Boats*, which is  $512 \times 512$ . The first column of the table shows BSNR values for observations  $z_j$ . In this table following numerical error values are presented: peak signal-to-noise ratio (PSNR) in dB,  $\text{PSNR} = 20 \log_{10}(\max_x |y(x)|/\text{RMSE})$ ; mean absolute error (MAE),  $\text{MAE} = \sum_x |y(x) - \hat{y}(x)|/n_1 n_2$ . As it is seen the quality of restoration is good and proves that the proposed technique is efficient for noisy data.

### 6.2 Restoration of color images

As a test image for blind deconvolution of color images we used  $256 \times 256$  RGB *Fruits* image (Fig.4c). We assume that blurring operator  $v_j$  for a single observation  $z_j = (R, G, B)$  is the same for all color  $R$  (red),  $G$  (green), and  $B$  (blue) channels. The PSFs  $v_j$  used are the same as for grayscale images experiments provided in the previous section. The level of noise is set to be 40 dB for each channel. The observations  $z_j$  obtained are illustrated in Fig.4d-f.

The natural approach to reconstruction is the use of (13)-(14) directly to these corrupted color channels separately. The parameter  $\Gamma$  for the ICI rule is fixed to be 0.9 for all color channels. The restored color image is shown (Fig.4a). The PSNR and MAE values are (34.7 33.3 32.5) and (3.21 3.83 4.49) for  $R$ ,  $G$ , and  $B$  color channels, respectively.

However, usually natural color images are highly correlated. We use the opponent color space transformation in order to decorrelate these color signals [12]:

$$\begin{bmatrix} I_1 \\ I_2 \\ I_3 \end{bmatrix} = \begin{bmatrix} 1/3 & 1/3 & 1/3 \\ 1/2 & 0 & -1/2 \\ 1/4 & -1/2 & 1/4 \end{bmatrix} \begin{bmatrix} R \\ G \\ B \end{bmatrix},$$

where  $I_1$  is one achromatic channel, and  $I_2, I_3$  are two opponent color channels.

As a result of color space transformation,  $I_1$  has higher SNR which makes problem of deconvolution easier, and  $I_2, I_3$  have lower SNR but image details, like edges and smooth areas, are emphasized more. Therefore, it is reasonable to use lower  $\Gamma$  for  $I_1$  in order to avoid oversmoothing and due to lower level of noise ( $\Gamma = 0.7$  in our experiments), and higher  $\Gamma$  for  $I_2, I_3$  to suppress noise as much as possible ( $\Gamma = 0.9$  and 1.0). The results of image restoration are illustrated in Fig.4b. The PSNR and MAE values are equal to (35.5 34.9 33.1) and (3.01 3.25 4.24), respectively for the channels  $R$ ,  $G$  and  $B$  of the image in the RGB color space. These PSNR values are about 1 dB higher than those for straightforward restoration in RGB color space.

It is worth to stress that the difference in visual quality evaluation is significant also. Comparison of Fig.4a and

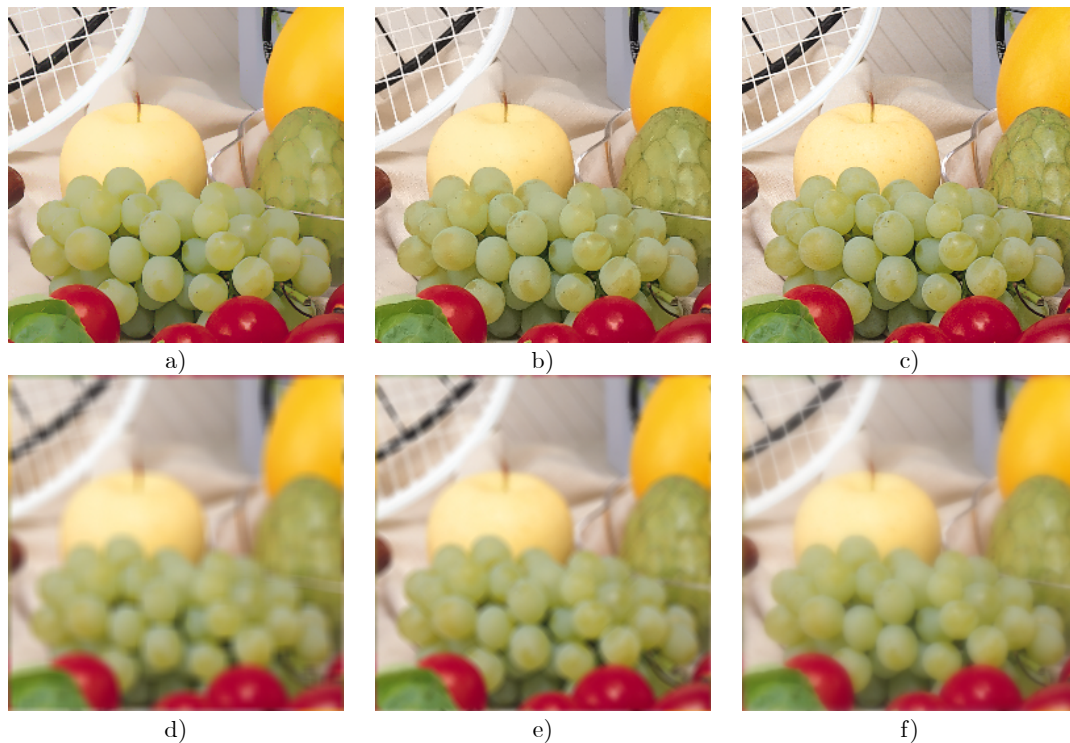


Figure 4: Blind reconstruction in RGB (a) and Opponent color space (b) of *Fruits* image (c) from 3 blurred noisy observations: d) blurred with boxcar  $9 \times 9$  PSF; e) blurred with rotated by  $45^\circ$  boxcar  $7 \times 7$  PSF; f) blurred with inverse-quadratic  $7 \times 7$  PSF.

Fig.4b clearly shows that 4b is more natural and tiny details are preserved very well.

The MATLAB implementation of the developed algorithms is available at <http://www.cs.tut.fi/~lasip/> to facilitate reproduction of results.

## 7. CONCLUSIONS

In this paper we propose an iterative multichannel blind deconvolution algorithm of noisy images. The incorporated denoising and regularization based on the spatially adaptive LPA-ICI technique. Simulations produced for both grayscale and color images show high quality of restoration in terms of objective numerical criteria and subjective visual evaluation.

## 8. ACKNOWLEDGMENTS

This work was supported by the Academy of Finland, project No. 213462 (Finnish Centre of Excellence program (2006 - 2011)). In part, the work of Dr. Vladimir Katkovnik is supported by *Visiting Fellow* grant from Nokia Foundation.

## REFERENCES

- [1] G. Harikumar and Y. Bresler, "Perfect blind restoration of images blurred by multiple filters: Theory and efficient algorithm," *IEEE Trans. Image Processing*, vol. 8, pp. 202–219, Feb. 1999.
- [2] G. Harikumar and Y. Bresler, "Exact image deconvolution from multiple FIR blurs," *IEEE Trans. Image Processing*, vol. 8, no. 6, pp. 846–862, 1999.
- [3] G. B. Giannakis and R. W. Heath Jr., "Blind identification of multichannel FIR blurs and perfect image restoration," *IEEE Trans. Image Processing*, vol. 9, pp. 1877–1896, 2000.
- [4] G. Panci, P. Campisi, S. Colonnese, and G. Scarano, "Multichannel blind image deconvolution using the bussgang algorithm: Spatial and multiresolution approaches," *IEEE Trans. Image Process.*, vol. 12, no. 11, pp. 1324–1337, 2003.
- [5] F. Sroubek and J. Flusser, "Multichannel blind iterative image restoration," *IEEE Trans. Image Process.*, vol. 12, no. 9, pp. 1094–1106, 2003.
- [6] F. Sroubek and J. Flusser, "Multichannel blind deconvolution of spatially misaligned images," *IEEE Trans. Image Process.*, vol. 14, no. 7, pp. 874–883, 2005.
- [7] L. Rudin, S. Osher, and E. Fatemi, "Nonlinear total variation based noise removal algorithms," *Phys. D*, vol. 60, pp. 259–268, 1992.
- [8] D. Mumford and J. Shah, "Optimal approximation by piecewise smooth functions and associated variational problems," *Commun. Pure Appl. Math.*, vol. 42, pp. 577–685, 1989.
- [9] T. Chan, S. Osher, J. Shen, "The digital TV filter and nonlinear denoising," *IEEE Trans. Image Processing*, vol. 10, no. 10, pp. 231–241, 2001.
- [10] V. Katkovnik, K. Egiazarian and J. Astola, "A spatially adaptive nonparametric image deblurring," *IEEE Transactions on Image Processing*, vol. 14, no. 10, pp. 1469–1478, 2005.
- [11] V. Katkovnik, K. Egiazarian, and J. Astola, "Adaptive window size image de-noising based on intersection of confidence intervals (ICI) rule", *Journal of Mathematical Imaging and Vision*, vol. 16, pp. 223–235, 2002.
- [12] K. N. Plataniotis, A. N. Venetsanopoulos, *Color Image Processing and Applications*, Springer-Verlag Berlin Heidelberg 2000.